Sexithiophene Adlayer Growth on Vicinal Gold Surfaces

Antti J. Mäkinen,* James P. Long, Neil J. Watkins, and Zakya H. Kafafi†

Naval Research Laboratory, 4555 Overlook Avenue, S.W., Washington, D.C. 20375

Received: November 5, 2004; In Final Form: January 26, 2005

We have investigated the initial stages of vacuum-deposited sexithiophene (α-6T) adlayer formation on Au(111) vicinal surfaces at room temperature. The in situ scanning tunneling microscopy (STM) and photoemission spectroscopy (PES) reveal a step edge-driven growth of α-6T on the Au(111) vicinal surfaces that first leads to the formation of an ordered monolayer, comprising two phases with the molecular major axes aligned along the step edges. The monolayer formation is then followed by the appearance of a single-phase 2D superstructure at a two-monolayer coverage. The results highlight the potential of using vicinal metal surfaces as templates for generating organized organic nanostructures over macroscopic areas for applications in organic electronics and moletronics.

I. Introduction

The desire to understand and to control the structure of organic molecular overlayers on metal surfaces has been driven by advances in organic electronics for the past 15 years. The performance of organic electronic and electro-optic devices such as organic field effect transistors,[1−3] photovoltaics,[4] and light emitting diodes[5] depends in a fundamental way on the molecular order, which affects the charge transport and the optical properties of thin film structures. More recently, interest in self-assembly based parallel processing techniques for generating organized nanostructures over macroscopic areas has been shaped by the development of moletronic structures where the functionality is defined by a single molecular entity and/or by its contact with a substrate.[6,7]

To achieve controlled growth of molecular layers on a metal surface, the use of an ordered substrate with large corrugation and anisotropy is desirable. The low index transition metal surfaces have been found to promote the ordered planar growth of many π-conjugated molecules, including oligothiophenes and their derivatives.[5,8−17] In particular, the corrugated (110) surfaces of Au, Ag, and Cu have been shown to drive anisotropic, ordered growth of sexithiophene (α-6T) films.[8,9,12,13] α-6T molecules align their major axes along the [1$\bar{1}$0] direction on the Au(110) surface,[8,9] whereas on the Ag(110) and Cu(110) surfaces, the molecules are oriented along the [001] direction.[12,13] The molecular alignment along principal crystal axes has been attributed to the anisotropy of these (110) transition metal surfaces arising from the missing-row reconstruction, where alternating rows of close-packed metal atoms along [001] are missing in the [1$\bar{1}$0] direction.

To pursue further the use of anisotropic metal surfaces as *templates*[18,19] for ordered molecular growth, we have investigated the initial stages of α-6T adlayer formation on Au(111) vicinal surfaces[20] at room temperature. The in situ scanning tunneling microscopy (STM) and photoemission spectroscopy (PES) reveal a step-edge driven growth of α-6T that first leads to the formation of an ordered monolayer, followed by 2D superstructure formation at a two monolayer coverage. The long-range order in the second monolayer is to a great extent due to the dual role of the first monolayer, which acts both as an alignment and as a buffer layer for the second. The buffer layer effect results in reduced molecule−substrate interaction in the second monolayer, enabling the α-6T molecules to adopt a single-phase superstructure. We expect this ability to control the adlayer−substrate interaction to provide new means for generating ordered molecular films on metal surfaces.

II. Experimental Section

The PES, including ultraviolet and X-ray photoemission spectroscopy (UPS, XPS), and the STM measurements were carried out in a UHV system (base pressure 5×10^{-11} Torr), consisting of preparation and analysis chambers separated by gate valves.

The single-crystal Au substrate (Accumet Materials Co.) was prepared by repeated cycles of Ar ion sputtering (0.5 keV) and annealing (680−720 K) before characterizing it by PES and STM. The α-6T (Oryza Laboratories, Inc.) was purified by train sublimation. Films of α-6T molecules were vacuum-deposited onto the Au substrate at a pressure of $\sim 8 \times 10^{-10}$ Torr. The average deposition rate, monitored with a quartz crystal oscillator, was 2−4 Å/min. After film deposition, the samples were moved from the preparation chamber to the analysis chambers without breaking vacuum.

STM was performed in a constant current mode at various substrate biases (V_s) at room temperature. Tungsten STM tips were prepared by electrochemical etching in 0.1 M NaOH solution. After placing the tips in a vacuum, they were Ar-ion sputtered (0.5 keV) for 20 min.

The HeI ($h\nu = 21.22$ eV) spectra of each deposited molecular adlayer were recorded at room temperature with a hemispherical energy analyzer for electron detection. The resolution of the analyzer was set to 50 meV. The sample was biased at −3.0 V to compensate for any contact potential between the sample and the analyzer. The XPS survey scans of the Au substrate were recorded with use of Al $K\alpha$ radiation ($h\nu = 1486.6$ eV) to verify a contamination-free surface.

III. Results

A. Bare Au Substrate. Large-scale STM images of the bare gold substrate, shown in Figure 1, indicate a nearly regular array

* Address correspondence to this author. E-mail: ajm@ccs.nrl.navy.mil.
† E-mail: kafafi@ccf.nrl.navy.mil.

10.1021/jp044921y CCC: $30.25
Published on Web 03/09/2005

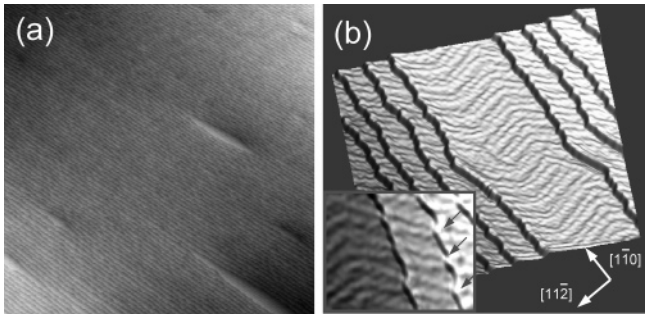

Figure 1. (a) Large scale (500 nm × 500 nm) topographic image of the Au(111) vicinal surface and (b) a detailed image of the same surface (75 nm × 75 nm) showing the reconstruction pattern and the propagation of the reconstruction lines across the steps. The inset shows the presence of step edge kinks where pairs of reconstruction lines cross a step (indicated by arrows). ($V_S = -50$ meV, $I = 0.5$ nA.)

of monatomic steps across the surface. In a few distinct locations at the surface, there are wider terraces, breaking up the otherwise mostly uniform vicinal surface. Apart from these "terrace defects", there are predominantly two Au(111) vicinal surface orientations, Au(788) and Au(11 11 12), as deduced from the 2D-Fourier analysis of the surface profile. Both vicinals evidently coexist within any particular STM image. The corresponding terrace widths (and miscut angles) are 3.8 (3.5°) and 5.8 nm (2.3°), respectively. The presence of these two distinct vicinal surfaces is not surprising, given their well-known stability.[18−20] A prominent feature of Figure 1b is the well-known 23 × $\sqrt{3}$ herring bone reconstruction pattern,[22,23] comprising parallel zigzag lines. This pattern is formed by a stress-induced surface contraction along the [1$\bar{1}$0] direction, perpendicular to the lines. The lines are ridges of surface atoms, occupying bridge sites, which separate fcc and hcp regions. The widths of the fcc and hcp regions are 3.8 and 2.5 nm, respectively. Consequently, the reconstruction lines appear in pairs defined by the narrower hcp region.[22−25] Note that the lines provide a convenient reference for the surface crystal orientation since they run along [11$\bar{2}$] and symmetry-related directions.

The average step direction runs roughly along [1$\bar{1}$0], as would be expected for a miscut defined by a sample normal tipped from [111] toward [11$\bar{2}$]. The departure of the average step direction from [1$\bar{1}$0] reflects a small azimuthal deviation from the ideal miscut angle. Important to the templating to be discussed, the reconstruction lines pass through the steps without displacement or change in direction. Nevertheless, there is a correlation between the reconstruction lines and the detailed structure of the steps, as the STM images reveal a tendency for a kink to occur where a pair of lines crosses a step (see the inset in Figure 1b). The kinks accommodate the miscut angle given the clear preference for the steps to run along the close-packed [1$\bar{1}$0]. The vicinal surfaces of Au(111), Au(788), and Au(11 11 12) are therefore "naturally" patterned in two dimensions: (i) perpendicular to the steps with a period equal to the terrace width (3.8 or 5.8 nm), determined by the miscut angle, and (ii) in the [1$\bar{1}$0] direction with a period of 6.3 nm, defined by the unit cell of the 23 × $\sqrt{3}$ herring bone reconstruction.[23]

B. Submonolayer Coverage of α-6T. At submonolayer coverage, the STM derivative image in Figure 2 reveals rodlike shapes along the step edges of the Au substrate. These shapes have an average width of 0.49 ± 0.05 nm and a predominant length of 5.0 ± 0.05 nm, as determined directly from the STM image. In some areas, the rods appear to be split into two shorter ones of half the length, ∼2.5 nm. The measured width and the shorter length compare well with the previously reported dimensions of the α-6T molecule, based on crystallographic data of single α-6T crystals[26] and STM measurements of α-6T molecules on a Si(100) surface.[27] It is therefore evident that two α-6T molecules arrange themselves end-to-end on a section of the step edge defined by the reconstruction lines, which are visible as shallow linear depressions, separating the narrow hcp region from the wider fcc region in the STM image of Figure 2. The 5-nm rods are oriented perpendicular to the reconstruction lines, implying their orientation along the [1$\bar{1}$0] direction. This clearly demonstrates the template effect of the stepped surface, which becomes even more evident at the one and two monolayer coverages.

We infer from the surface profile of the 3D rendering of the STM image in Figure 2b that the α-6T molecules are located at the bottom of the step risers. While we are aware that variations in the density of states can complicate determination of STM height profiles, our interpretation of the location of the α-6T molecules is supported by the rest of our experimental results and analysis (see Sections IIIE and IVA). Interestingly, the bottom of the step risers is the only location anywhere on the vicinal surface where we were able to obtain images of the molecules at submonolayer coverage. This observation does not necessarily exclude the presence of the α-6T elsewhere on the surface but rather implies a fast diffusion of the molecules at room temperature preventing their stable imaging away from the step edges.

Although single molecules are observed in a few places along the step edges, the molecular substructure of α-6T proves to be more elusive. Only three bright spots are seen on the single molecules instead of six as expected for the six thiophene moietites of an α-6T molecule (discussed further in Section IV).

C. One Monolayer Coverage of α-6T. For a single monolayer coverage, the STM image in Figure 3a reveals a well-organized adlayer that follows the topology of the stepped Au substrate. The measured step height is ∼0.3 nm, in reasonable agreement with the expected height, 0.23 nm, of a monatomic step of the Au(111) surface. A notable feature of the α-6T-covered steps is the periodic form of their edges. The repeat unit comprises a ∼5 nm straight segment, making a 60° angle with a shorter segment. The periodicity along the edge, as defined by two consecutive edge kinks and measured in the direction of the 5 nm segment, is 6.3 nm, equal to the combined length of the fcc and the hcp regions of the 23 × $\sqrt{3}$ Au reconstruction as indicated in Figure 3a.

The α-6T monolayer exhibits two different phases, associated with the orientation of two step-edge segments. In Phase I, the α-6T molecules appear to line up as two-molecule-long chains parallel to the 5-nm-long edge segment. Phase II is associated with the shorter edge segment, and at least the molecules near the step edge seem to be parallel to the shorter segment. However, the molecules at the center of the terrace are not clearly resolved. Based on the line scan shown in Figure 3b, the separation of the molecules in Phase I is fairly uniform, 0.57 ± 0.05 nm. However, the height profile also reveals corrugation between pairs of the chains. The depth of the valley between adjacent pairs is 0.03 nm deeper than the valley between molecular chains within a pair, implying a higher charge density between the molecules within a pair (see the height profile in Figure 3b).

The surface profile in Figure 3b also indicates that molecules at the upper step edge are located 0.24 nm higher than the

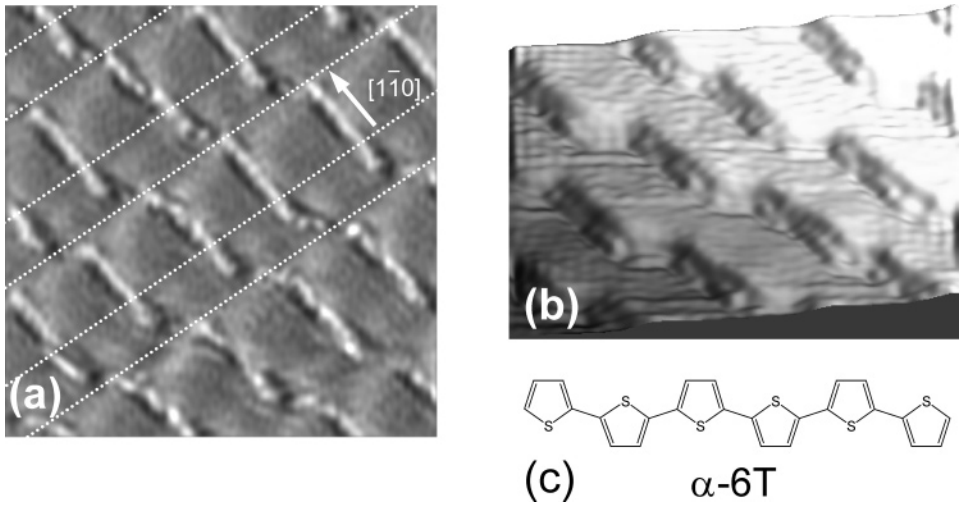

Figure 2. (a) STM derivative image (20 nm × 20 nm) of a submonolayer coverage of α-6T on the Au vicinal surface where dashed lines indicate the position and direction of reconstruction lines, (b) 3D rendering of the same coverage (20 nm × 16 nm) ($V_S = -1.7$ V, $I = 0.5$ nA), and (c) the chemical structure of α-6T.

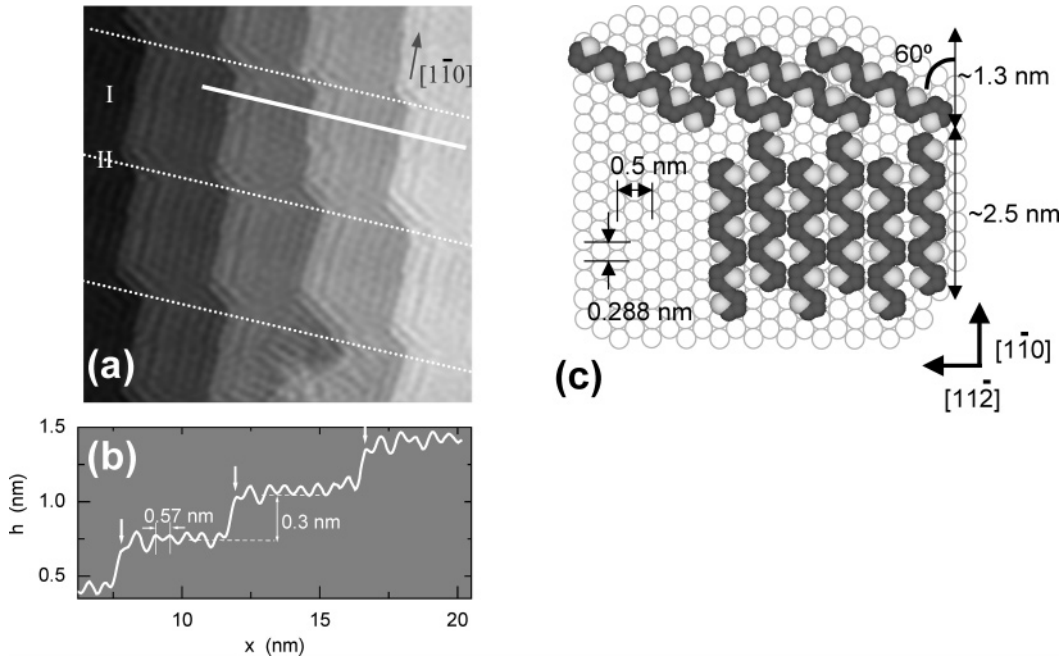

Figure 3. (a) High-resolution topographic image (20 nm × 20 nm) of the 1 ML α-6T coverage on the Au vicinal surface (superimposed dashed lines run perpendicular to the [1$\bar{1}$0] direction separated by 6.3 nm, indicating the repeat length of Au 23 × $\sqrt{3}$ surface reconstruction ($V_S = -1.0$ V, $I = 0.5$ nA)), (b) surface profile of the 1 ML coverage (indicated by the solid white line in the image) with vertical arrows showing the positions of molecules at step edges, and (c) the proposed ML structure. Note that the α-6T molecules are *incommensurate* with the Au atom positions.

molecules on the lower terrace, but 0.07 nm lower than the other molecules on the upper terrace.

D. Two Monolayer Coverage of α-6T. The deposition of the second monolayer produces a remarkably ordered single phase of α-6T that follows the topology of the stepped Au substrate (step height ~0.25 nm). The STM image in Figure 4b reveals molecules tightly packed side-by-side and organized as *cells* whose lateral and longitudinal dimensions are defined by the step width (*W*) and by the length of the α-6T molecule (*L*), respectively. The width and the length of α-6T molecules in these cells, as determined from the STM image, are 0.57 ± 0.05 nm and 2.5 ± 0.05 nm, respectively. The submolecular structure of α-6T is also resolved in most of the image: the molecular "rods" are found to comprise six bright spots corresponding to the thiophene units of the α-6T chain.

The most striking feature of the second monolayer is that all the cells and therefore all the sexithiophene molecules are oriented in the same direction, along [1$\bar{1}$0]. In addition, the cells are organized in well-defined rows, perpendicular to the [1$\bar{1}$0] direction. This gives rise to a *2D superstructure* of the second α-6T monolayer, defined by the cell parameters *W* and *L*.

E. PES of α-6T Adlayer Formation. Further evidence for a well-ordered bare Au surface is provided by the HeI spectrum shown in Figure 5. The low binding energy portion of the spectrum shows a strong feature, located between ~0.5 eV and the Fermi level, which is derived from the widely reported, Shockley-type, Au(111) surface state (SS), lying in the projected sp-band gap around the center of the surface Brillouin zone.[28] For vicinal surfaces, this SS maintains its free-particle like character only in the direction parallel to the steps. In the perpendicular direction, the electron wave function is confined, leading to the appearance of discrete one-dimensional quantum well states.[29−31] Although not explicitly resolved, the presence

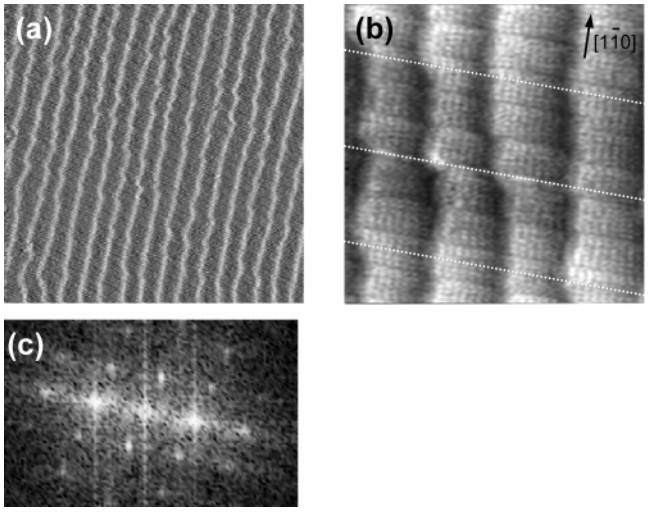

Figure 4. (a) STM derivative image (75.8 nm × 75.8 nm) of the Au vicinal with a 2 ML coverage of α-6T, (b) high-resolution topographic image (20 nm × 20 nm) of the same coverage where the α-6T cells are clearly defined by the molecular length (*L*) and by the terrace width (*W*) (superimposed dashed lines run perpendicular to the [1$\bar{1}$0] direction separated by 6.3 nm, indicating the repeat length of Au 23 × $\sqrt{3}$ surface reconstruction), and (c) Fourier transform of the 75.8 nm × 75.8 nm image. The long-range order is indicated by the appearance of the second order peak in the directions of both principal axes (V_S = −1.0 V, I = 0.25 nA).

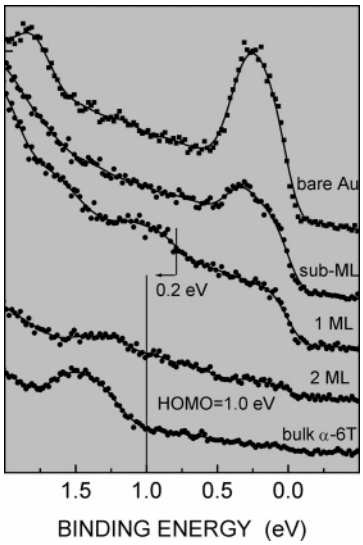

Figure 5. HeI spectra of the α-6T/Au interface as the thickness of the molecular layer is increased. The binding energy is referenced to the Fermi level of the Au substrate.

of the quantum well states[32] in the surface state feature in Figure 5 is suggested by its asymmetric line shape.

The HeI spectrum of the partial α-6T coverage of the Au substrate exhibits a significantly decreased intensity for the Au SS, as is commonly induced by adlayer molecules. Although the coverage *up to* the first monolayer could not be quantified with STM, the completion of the first monolayer is evidenced by the HeI spectrum when the SS feature in the PES spectrum has completely disappeared, indicating complete depopulation of the SS by the organic adlayer. While the density of the states right below the Fermi level appears flat, a small intensity increase is observed at 1.0 eV, which is attributed to the appearance of the frontier orbitals of α-6T.

As the α-6T coverage is increased to two monolayers, the Fermi level remains visible, albeit with a 4-fold reduction in intensity, and provides a valid reference. The highest occupied molecular orbital (HOMO) feature in the spectrum shifts 0.2 eV toward higher binding energy. This higher binding energy position of the HOMO remains the same within the estimated error, ±0.1 eV, up to the bulk thicknesses of α-6T, as indicated in Figure 5. The shift of the HOMO between the first and second monolayers is attributed to final state effects that have been discussed recently elsewhere.[33]

IV. Discussion

A. α-6T Adsorption at Step Edges. The initial attachment of α-6T molecules at the bottom of the monatomic Au steps implies higher adsorption energy for the sites near the bottom of the step edge than anywhere else on the Au surface. It is well-known that surface defects, such as dislocations, vacancies, and steps, often provide preferential adsorption sites.[34] The alteration of the lattice symmetry at the defect sites leads to positive (negative) changes in the adsorption energy, which is thought to result from the increase (decrease) in the coordination number of adsorbates at these sites.[14,34]

To elucidate the actual mechanism responsible for the adsorption energy of the step edge sites it is useful to consider the chemical character of the α-6T/Au interface. Both quantum chemical calculations and XPS measurements indicate the absence of strong chemical interaction between oligo- and polythiophenes and gold.[45,46] The inertness of the α-6T/Au interface is also demonstrated by the positions of the α-6T HOMO and the lowest unoccupied molecular orbital (LUMO), measured by PES (this study) and inverse photoemission spectroscopy (IPES),[47] respectively. The HOMO and the LUMO are found to be located 0.8−1.0 and 1.3 eV below and above the Au Fermi level, respectively, making charge transfer (CT) between α-6T and Au unlikely. Furthermore, neither UPS nor IPES show the appearance of gap states at the α-6T/Au interface, which is consistent with very weak or nonexistent CT between the organic and the metal.[48] As a consequence of weak chemical interaction at the α-6T/Au interface, the enhancement of surface CT by the redistribution of the electron density at steps, known as Smoluchowski smoothing,[35] is likely to be insignificant.[14,15,36]

In the absence of evidence for strong chemical interaction, we expect the α-6T adsorption at Au steps to be determined mostly by physisorptive processes. More specifically, the adsorption energy of surface sites depends partly on the local density of states (LDOS) of these sites. The LDOS is affected by (i) perturbations due to adsorbates and by (ii) SS electron scattering, also known as Friedel oscillations.[16,17] Both types of interaction are dominated by the SS electrons residing immediately outside the metal (111) surface. The SS electrons are expected to have a pronounced influence on the repulsive part of the physisorption potential through the short-ranged Pauli repulsion, which depends on the charge density in front of the surface.[40−43] The direct consequence of the increased repulsive potential is weakened physisorption. Conversely, surface defects, including adsorbates themselves, can act as repulsive scattering centers for the 2-D surface-state electron gas, leading to the local depopulation of the surface state in the vicinity of such defects. Consequently, the surface attachment of the adsorbate is strengthened as the surface state depopulation induces an effective attractive interaction between the adsorbates.[41,43,44]

The observed SS depopulation in HeI spectra suggests that the initial accumulation of α-6T molecules at the bottom of the Au steps may be partly due to the perturbations of LDOS of the surface electrons and the resulting attractive interaction between the bottom edge and the molecules. Also, it has been

argued that the step of Au(111) may reduce the LDOS of the SS band, making the SS density oscillations less pronounced near the bottom of the steps.[37−39,49] The reduced SS density at the bottom of the steps would therefore lead to a decrease in the repulsive part of the potential, making the sites near the bottom edge more attractive for adsorption.

B. Effect of Step Structure on Monolayer Formation. The α-6T/Au monolayer in Figure 3 is reminiscent of a "raft" of molecules within which the packing of the molecules is optimized in order to maximize the coverage of the Au vicinal surface as evidenced by the two phases identified on the Au terraces. On the basis of the STM image of the α-6T/Au monolayer, we propose a two-phase model structure for the one monolayer coverage shown in Figure 3c. The orientation of the molecules in Phase I is determined by the step edge in the $[1\bar{1}0]$ direction, which is also the nearest neighbor (NN) direction on the (111) surface. The molecules in Phase II align themselves along another NN axis, as determined by the shorter edge segment, making a 60° angle to the $[1\bar{1}0]$ direction. In the model, the molecules in Phase II have been rigidly shifted with respect to each other according to the rationalization of the STM images. The projection of the length of an α-6T molecule onto the $[1\bar{1}0]$ direction is 1.25 nm (=2.5 cos(60°) nm), which is close to the length of Phase II (1.3 nm) in the $[1\bar{1}0]$ direction.

The distance between the adjacent thiophene rings of an α-6T molecule is ∼0.4 nm whereas the NN distance on Au(111) is 0.288 nm. Therefore, we conclude that the packing of the molecules in the $[1\bar{1}0]$ direction is *incommensurate* with the underlying Au(111) lattice. Similarly, the spacing between parallel chains of α-6T molecules is 0.57 nm while the distance between the adjacent rows of Au atoms parallel to $[1\bar{1}0]$ is 0.25 nm, implying incommensurate packing also in the $[11\bar{2}]$ direction. This is in contrast to recent reflection high energy electron diffraction (RHEED) measurements reported by Yoshikawa et al.[12] on α-6T adlayer formation on Ag(111) surfaces, where the molecules were proposed to pack *commensurately* with the bridge sites in the $[1\bar{1}0]$ direction. The authors found the characteristic spacing in the $[11\bar{2}]$ direction to be 0.646 nm on the α-6T-covered Ag(111) surface, implying that the α-6T molecules form chains parallel to $[1\bar{1}0]$.[12] Since the difference in lattice constants of Au(111) and Ag(111) surfaces (2.9%) is not sufficient to explain the larger spacing of molecules in the $[11\bar{2}]$ direction on the Ag(111) surface we conclude that the α-6T molecules pack differently on these two (111) surfaces. One possible explanation is a proposed charge transfer between α-6T and the more reactive silver surface, evidenced by the chemical shift of the S(1s) peak in the XPS of the α-6T/Ag interface.[12]

Since the packing of the α-6T molecules is incommensurate with respect to the atomic positions of the Au(111) surface, it can be concluded that the vicinal structure (steps) and the intermolecular interaction have a significant role in the monolayer formation. After the initial nucleation, promoted by the step edges, molecule−molecule interactions and/or adsorbate-induced surface electronic perturbations are expected to contribute considerably to ordering the first layer of molecules.[14] There is a potential hint about an aspect of this interaction in the line scan of the STM topograph in Figure 3. As noted earlier, the lower depth of the valley between molecular chains implies a correlation between the adjacent chains in Phase I. In the model for the monolayer structure included in Figure 3c, the correlation between the molecules is illustrated by the registry of the sulfur atoms on the adjacent molecular strands. This registry has been achieved by shifting the molecules by one thiophene unit along their long axis. Although the proposed model is phenomenological at its best, it is consistent with additional charge density between paired molecules (see Section IIIC), as observed in this study, and also with the previously reported monolayer structures of α-6T on Au(110) surfaces.[8]

The close-packed structure of the first monolayer appears to be altered for molecules adsorbed at the upper step edge as indicated by the surface profile in Figure 3b. These step edge molecules may indicate a special adsorption site at the step edge, analogous to those found for C_{60} molecules adsorbed on a Au(111) surface.[50] Because of their elevated position with respect to the monolayer surface on the lower terrace these step edge molecules may affect the formation of the second monolayer, should the growth of the second layer proceed from the step edges.

The STM images of areas adjacent to the edge kinks have topologies which are reminiscent of interference patterns. In fact, interference effects, such as Moiré patterns, have been observed for molecular overlayers on metal surfaces.[8,14,51] At appropriate tunneling distances, the superposition of the substrate lattice and the overlayer structure can create a Moiré pattern, which is typically observed as a line pattern with a longer periodicity than those of the substrate or the adlayer. Additionally, end-to-end arrangement of molecules in a monolayer has been shown to lead to interference contributions in the tunneling current.[51] The interference between the metal surface and the adlayer molecules may also explain the absence of well-resolved submolecular structure in the image of the step-edge attachment of α-6T in Figure 2. On the other hand, the substructure of the α-6T molecules is better observed in the second monolayer (see Figure 4b) where molecules are further away from the Au substrate, and consequently, the interference effects are likely reduced.

C. 2D Superstructure Formation. The influence of the substrate in templating layers beyond the first monolayer is an important issue for engineering structured molecular overlayers. For the case of α-6T on vicinal gold, the single orientational phase of the second monolayer (Figure 4) exhibits features imposed both by the underlying structure and by a significant intralayer interaction that favors a side-by-side molecular organization, enhancing long-range order. The influence of the underlying substrate is evident in Figure 4 by the steps running predominantly along $[1\bar{1}0]$, as also observed in the images of bare Au and the first monolayer. In addition, there are regions where kinks occur quasiperiodically along a step edge with a separation commensurate with the underlying periodicity of the herringbone reconstruction. (This can be seen in Figure 4b, where dotted lines spaced by the 6.3-nm reconstruction periodicity are overlaid as guides to the eye.) Note that unlike the first monolayer, where shorter step segments guided a second orientational phase, the cell structure of the second monolayer is not pinned to any given kink.

The first monolayer appears to act partly as an alignment layer and partly as a buffer layer so that the molecular packing in the second monolayer is most sensitive only to the gross features of the underlying step structure. Consequently, the molecular packing in the first and second monolayers is resolved differently, resulting in the two first monolayers being incommensurate with each other. This leads to the unidirectional ordering of the rectangular cells in the 2D superstructure, where the cell dimensions are determined by the long axis of α-6T and by the terrace width. The obtained structure is in contrast to superstructures formed by depositing a submonolayer of Co atoms onto a Au(788) vicinal surface.[19] In this previous study,

the cells in the superstructure were defined by the separation of the reconstruction lines and the step width. The use of more sizable rodlike molecules therefore offers additional control over the cell parameters.

Despite the impressive long-range order displayed by the superstructure of the second monolayer of α-6T (indicated by the second order peak in the Fourier transform of the STM image in Figure 4c), the coherence length of the superstructure can be limited significantly by the inhomogeneous terrace width. This is evident from Figure 4 where the STM image shows the effective cell width varying from 3.6 to 5.7 nm. Clearly, the biggest challenge in utilizing vicinal surfaces as templates for 2D nanostructures is the selection of a stable vicinal structure and its correct preparation. In the present case, the largest defect-free area (i.e., an area without a wider terrace) found on the bare substrate was ∼300 nm × 300 nm (see Figure 1).

V. Conclusion

The combined PES and STM study of the α-6T adlayer formation on Au(111) vicinal surfaces has highlighted the effects of stepped surface on the molecular order. The sites at the bottom of the Au steps promote the growth of the α-6T overlayer, where the attractive interaction between the step edge and the molecules is attributed to the high coordination number and the modulation of the LDOS of surface electrons. The step edges, therefore, have an important role in the formation of the first monolayer, comprising two phases with the molecular major axis aligned along the step edges. At the two-monolayer thickness, the α-6T molecules form a 2D superstructure, where the cell dimensions are defined by the length of the molecules and by the width of the Au(111) step. The biggest challenge in using vicinal metal surfaces for generating organized organic nanostructures appears to be the preparation of the stepped surface, which is found to be the limiting factor for the coherence length of the 2D superlattice.

Acknowledgment. This research was funded by ONR.

References and Notes

(1) Dimitrakopolous, C. D.; Mascaro, D. J. *IBM J. Res., Dev.* **2001**, *45*, 11.
(2) Torsi, L.; Dodabalapur, A.; Rothberg, L. J.; Fung, A. W. P.; Katz, H. E. *Science* **1996**, *272*, 1462.
(3) Nichols, J. A.; Gundlach, D. J.; Jackson, T. N. *Appl. Phys. Lett.* **2003**, *83*, 2366.
(4) Gregg, B. A. *J. Phys. Chem. B* **2003**, *107*, 4688.
(5) Forrest, S. R. *Chem. Rev.* **1997**, *97*, 1793.
(6) Chen, J.; Reed, M. A.; Rawlett, A. M.; Tour, J. M. *Science* **1999**, *286*, 1550.
(7) Nitzan, A.; Ratner, M. A. *Science* **2003**, *300*, 1384.
(8) Parato, S.; Floreano, L.; Cvetko, D.; De Renzi, V.; Morgante, A.; Modesti, S.; Biscarini, F.; Zamboni, R.; Taliani, C. *J. Phys. Chem. B* **1999**, *103*, 7788.
(9) Buongiorno Nardelli, M.; De Renzi, V.; Floreano, L.; Gotter, R.; Morgante, A.; Peloi, M.; Tammasini, F.; Danieli, R.; Rossini, S.; Taliani, C.; Zamboni, R. *Phys. Rev. B* **1996**, *53*, 1095.
(10) Soukopp, A.; Glöckler, K.; Kraft, P.; Schmitt, S.; Sokolowski, M.; Umbach, E.; Mena-Osteritz, E.; Bäuerle, P.; Hädicke, E. *Phys. Rev. B* **1998**, *58*, 13882.
(11) Kilian, L.; Weigand, W.; Umbach, E.; Langner, A.; Sokolowski, M.; Meyerheim, H. L.; Maltor, H.; Cowie, B. C. C.; Lee, T.; Bäuerle, P. *Phys. Rev. B* **2002**, *66*, 075412.
(12) Yoshikawa, G.; Kiguchi, M.; Ikeda, S.; Saiki, K. *Surf. Sci.* **2004**, *559*, 77.
(13) Kiguchi, M.; Entani, S.; Saiki, K.; Yoshikawa, G. *Appl. Phys. Lett.* **2004**, *84*, 3444.
(14) Pascal, J. I.; Jackiw, J. J.; Kelly, K. F.; Conrad, H.; Rust, H.-P.; Weiss, P. S. *Phys. Rev. B* **2000**, *62*, 12632.
(15) Sykes, E. C. H.; Han, P.; Weiss, P. S. *J. Phys. Chem. B* **2003**, *107*, 5016.
(16) Stranick, S. J.; Kamna, M. M.; Weiss, P. S. *Science* **1994**, *266*, 99.
(17) Stranick, S. J.; Kamna, M. M.; Weiss, P. S. *Surf. Sci.* **1995**, *338*, 41.
(18) Repain, V.; Berroir, J. M.; Rousset, S.; Lecoeur, J. *Surf. Sci.* **2000**, *447*, L152.
(19) Repain, V.; Baudot, G.; Ellmer, H.; Rousset, S. *Europhys. Lett.* **2002**, *58*, 730.
(20) Rousset, S.; Repain, V.; Baudot, G.; Garreau, Y.; Lecoeur, J. *J. Phys.*: *Condens. Matter* **2003**, *15*, S3363.
(21) Frank, E. R.; Chen, X. X.; Hamers, R. J. *Surf. Sci.* **1995**, *334*, L709.
(22) Harten, U.; Lahee, A. M.; Peter Toennies, J.; Wöll, Ch. *Phys. Rev. Lett.* **1985**, *54*, 2619.
(23) Wöll, Ch.; Chiang, S.; Wilson, R. J.; Lippel, P. H. *Phys. Rev. B* **1989**, *39*, 7988.
(24) Barth, J. V.; Brune, H.; Ertl, G.; Behm, R. J. *Phys. Rev. B* **1990**, *42*, 9307.
(25) Chen, W.; Madhavan, V.; Jamneala, T.; Crommie, M. F. *Phys. Rev. Lett.* **1998**, *80*, 1469.
(26) Horowitz, G.; Bachet, B.; Yasser, A.; Lang, P.; Demanze, F.; Fave, J.-L.; Garnier, F. *Chem. Mater.* **1995**, *7*, 1337.
(27) Lin, R.; Galili, M.; Quaade, U. J.; Brandbyge, M.; Børnholm, T.; Degli Esposti, A.; Biscarini, F.; Stokbro, K. *J. Chem. Phys.* **2002** *117*, 321.
(28) Kevan, S. D.; Gaylord, R. H. *Phys. Rev. B* **1987**, *5809.*
(29) Mugarza, A.; Mascaraque, A.; Perez-Dieste, V.; Repain, V.; Rousset, S.; Garcia de Abajo, F. J.; Ortega, J. E. *Phys. Rev. Lett.* **2001**, *87*, 107601.
(30) Mugarza, A.; Mascaraque, A.; Repain, V.; Altmann, K. N.; Himpsel, F. J.; Koroteev, Y. M.; Chulkov, E. V.; Rousset, S.; Garcia de Abajo, F. J.; Ortega, J. E. *Phys. Rev. B* **2002**, *66*, 245419.
(31) Mugarza, A.; Ortega, J. E.; Himpsel, F. J.; Garcia de Abajo, F. J. *Phys. Rev. B* **2003**, *67*, 081404.
(32) There are two quantum well energy levels for the surface state on the Au(788) vicinal, 0.40 and 0.11 eV,[29] and three on the Au(23 23 21) vicinal, 0.420, 0.250, and 0.055 eV.[30]
(33) Hill, I. G.; Mäkinen, A. J.; Kafafi, Z. H. *J. Appl. Phys.* **2000**, *88*, 889.
(34) Wandelt, K. *Surf. Sci.* **1991**, *251/252*, 387.
(35) Smoluchowski, R. *Phys. Rev.* **1941**, *60*, 661.
(36) The adsorption of molecules on electron-rich or -deficient regions due to Smoluchowski smoothing is expected to enhance the CT surface/molecular bond near the steps, where nucleophilic and electrophilic molecules have been shown to accumulate first on the top and on the bottom of the steps, respectively.[14,15]
(37) Hasegawa, Y.; Avouris, Ph. *Phys. Rev. Lett.* **1993**, *71*, 1071.
(38) Avouris, Ph.; Lyo, I.-W.; Molinas-Mata, P. *Chem. Phys. Lett.* **1995**, *240*, 423.
(39) Avouris, Ph.; Lyo, I.-W. *Science* **1994**, *264*, 942.
(40) Memmel, N.; Bertel, E. *Phys. Rev. Lett.* **1995**, *75*, 485.
(41) Bertel, E. *Surf. Sci.* **1995**, *331*−*331*, 1136.
(42) Bertel, E. *Surf. Sci.* **1996**, *367*, L61.
(43) Bertel, E. *Surf. Sci. Rep.* **1998**, *32*, 91.
(44) Zeppenfeld, P.; Horch, S.; Comsa, G. *Phys. Rev. Lett.* **1994**, *73*, 1259.
(45) Lachkar, A.; Selmani, A.; Leclerc, E.; Mokhliss, R. *Synth. Met.* **1994**, *66*, 209.
(46) Elfeninat, F.; Fredriksson, C.; Sacher, E.; Selmani, A. *J. Chem. Phys.* **1995**, *102*, 6153.
(47) Hill, I. G.; Kahn, A.; Soos, Z. G.; Pascal, R. A., Jr. *Chem. Phys. Lett.* **2000**, *327*, 181.
(48) Hill, I. G.; Schwartz, J.; Kahn, A. *Org. Electron.* **2000**, *1*, 5.
(49) Charge density fluctuations (or Friedel oscillations) associated with surface state electron scattering[37,39] have been found to affect molecule-to-surface attachment on the terraces of transition metal (111) surfaces.[15,17] However, all the observations of the interaction between charge density extrema and adlayer molecules have been made exclusively at low temperatures, 4−77 K. This is consistent with the estimates for the relatively low binding energies associated with the density oscillations, e.g., ∼15 meV on Cu(111).[40]
(50) Rogero, C.; Pascual, J. I.; Gomez-Herrero, J.; Baro, A. M. *J. Chem. Phys.* **2002**, *116*, 832.
(51) Marchenko, A.; Lukyanets, S.; Cousty, J. *Phys. Rev. B* **2002**, *65*, 045414.